Rev. Colomb. Cienc. Quím. Farm., **54**(1), 218–230 (2025)

Scientific research article

Antiviral effect of anthocyanins in vegetables and fruits against viral diseases: Insight to medication design by computational chemistry approaches

Fatemeh Mollaamin[1]* & Majid Monajjemi[2]

[1] Department of Biomedical Engineering, Faculty of Engineering and Architecture, Kastamonu University, Kastamonu, Turkey.

[2] Department of Chemical Engineering, Central Tehran Branch, Islamic Azad University, Tehran, Iran.

*Corresponding author E-mail: fmollaamin@kastamonu.edu.tr

Received: April 19, 2024
Corrected: January 30, 2025
Accepted: February 6, 2025

https://doi.org/10.15446/rcciquifa.v54n1.119556

SUMMARY

Introduction: The probe for ideal medications with absolute antiviral activity against SARS-CoV-2 is still in place, and attention has been recently drawn to medicinal plants. **Aims:** To evaluate the several molecular targets as points of therapeutic intervention. **Methods:** Clusters of metal ions of Mg^{2+}, Al^{3+}, Ga^{3+}, Sn^{2+}, Cr^{3+}, Fe^{3+} joined to anthocyanins in water media were studied for unraveling the color shifting of different complexes of these structures in the low ranges of pH using DFT/B3LYP/6–31G (d,p) method. **Results:** It has been studied the metal cations diffusing of deprotonating for the anthocyanin (B)-ring of Mal, Peo, Del, Pet, Cya in water and applying the IR method for getting the physico-chemical specifications of intensity, frequency, and absorbance of the compounds, respectively. It has been seen that by increasing the pH, the frequency of Al^{3+}Cya, Ga^{3+}Cya, Mg^{2+}Cya complexes increase between pH ≈1.1-1.5. The change in Gibbs free energy change (ΔG) may be the best indicator of the protection offered by dietary stabilizers on anthocyanins, which demonstrated the best stabilizer among dietary compounds as Del with $\Delta G = -2.92\times10^{-5}$ kcal/mol. Furthermore, the partial charges and spin density have been gained by matching the electrostatic potential to atomic charge of O^{+}_{17}, O^{+}_{16}, and O^{+}_{7} ions for M^{n+}(31)Cya, M^{n+}(32)Del and M^{n+}(35)Pet, respectively. **Conclusions:** The anthocyanins discussed in this article indicate robust binding affinities and strong inhibitory molecular interactions with the target proteins and could be well exploited as potential medication candidates with potent multiple antiviral impacts against COVID-19 virus.

Keywords: COVID-19; anthocyanins; ion chelation; DFT.

RESUMEN

Efeito antiviral de antocianinas em vegetais e frutas contra doenças virais: uma visão do projeto de medicamentos por meio de abordagens de química computacional

Introducción: La investigación de medicamentos ideales con actividad antiviral absoluta contra el SARS-CoV-2 aún está en marcha, y recientemente se ha llamado la atención sobre las plantas medicinales. **Objetivos:** Evaluar los diversos objetivos moleculares como puntos de intervención terapéutica.

Métodos: Se estudiaron grupos de iones metálicos de Mg^{2+}, Al^{3+}, Ga^{3+}, Sn^{2+}, Cr^{3+}, Fe^{3+} unidos a antocianinas en medios acuosos para desentrañar el cambio de color de diferentes complejos de estas estructuras en los rangos bajos de pH utilizando el método DFT/B3LYP/6–31G (d,p). **Resultados:** Se ha estudiado la difusión de cationes metálicos de desprotonación para el anillo de antocianina (B) de Mal, Peo, Del, Pet, Cya en agua y se ha aplicado el método IR para obtener las especificaciones fisicoquímicas de intensidad, frecuencia y absorbancia de los compuestos, respectivamente. Se ha visto que al aumentar el pH, la frecuencia de los complejos Al^{3+}Cya, Ga^{3+}Cya, Mg^{2+}Cya aumenta entre pH ≈1,1-1,5. El cambio en el cambio de energía libre de Gibbs (ΔG) puede ser el mejor indicador de la protección ofrecida por los estabilizadores dietéticos sobre las antocianinas, que demostraron ser el mejor estabilizador entre los compuestos dietéticos como Del con $\Delta G = -2.92\times10^{-5}$ kcal/mol. Además, las cargas parciales y la densidad de espín se han obtenido al hacer coincidir el potencial electrostático con la carga atómica de los iones $O^{+}{}_{17}$, $O^{+}{}_{16}$ y $O^{+}{}_{7}$ para M^{n+}(31)Cya, M^{n+}(32)Del y M^{n+}(35)Pet, respectivamente. **Conclusiones:** Las antocianinas analizadas en este artículo indican afinidades de unión robustas y fuertes interacciones moleculares inhibitorias con las proteínas objetivo y podrían ser bien explotadas como posibles candidatos a medicamentos con potentes impactos antivirales múltiples contra el virus COVID-19.

Palavras-chave: COVID-19; antocianinas; quelación iónica; DFT.

RESUMO

Efecto antiviral de las antocianinas en verduras y frutas contra enfermedades virales: información sobre el diseño de medicamentos mediante enfoques de química computacional

Introdução: A sonda para medicamentos ideais com atividade antiviral absoluta contra SARS-CoV-2 ainda está em andamento, e a atenção foi recentemente atraída para plantas medicinais. **Objetivos:** Avaliar os vários alvos moleculares como pontos de intervenção terapêutica. **Métodos:** Clusters de íons metálicos de Mg^{2+}, Al^{3+}, Ga^{3+}, Sn^{2+}, Cr^{3+}, Fe^{3+} unidos a antocianinas em meio aquoso foram estudados para desvendar a mudança de cor de diferentes complexos dessas estruturas nas baixas faixas de pH usando o método DFT/B3LYP/6–31G (d,p). **Resultados:** Foi estudada a difusão de cátions metálicos de desprotonação para o anel de antocianina (B) de Mal, Peo, Del, Pet, Cya em água e aplicando o método IR para obter as especificações físico-químicas de intensidade, frequência e absorbância dos compostos, respectivamente. Foi observado que ao aumentar o pH, a frequência dos complexos Al^{3+}Cya, Ga^{3+}Cya, Mg^{2+}Cya aumenta entre pH ≈1,1-1,5. A mudança na mudança de energia livre de Gibbs (ΔG) pode ser o melhor indicador da proteção oferecida pelos estabilizadores dietéticos em antocianinas, que demonstraram o melhor estabilizador entre os compostos dietéticos como Del com $\Delta G = -2.92\times10^{-5}$ kcal/mol. Além disso, as cargas parciais e a densidade de spin foram obtidas ao combinar o potencial eletrostático com a carga atômica dos íons $O^{+}{}_{17}$, $O^{+}{}_{16}$ e $O^{+}{}_{7}$ para M^{n+}(31)Cya, M^{n+}(32)Del e M^{n+}(35)Pet, respectivamente. **Conclusões:** As antocianinas discutidas neste artigo indicam afinidades de ligação robustas e fortes interações moleculares inibitórias com as proteínas alvo e podem ser bem exploradas como potenciais candidatos a medicamentos com múltiplos impactos antivirais potentes contra o vírus COVID-19.

Palabras clave: COVID-19; antocianinas; quelação iônica; DFT.

1. INTRODUCTION

A recent pathogen severe acute respiratory syndrome coronavirus 2 (SARS-CoV-2) has spread worldwide and become pandemic with thousands new deaths and infected cases globally [1–6]. Natural drugs and herbs with their anti-inflammatory properties might have pleiotropic functions in COVID-19 treatment [7–11]. Some antibodies extracted from plants are supposed to answer very quickly to the emergence of recent variants of COVID-19 [12–19]. Anthocyanins are one of the four subclasses of Flavonoids which represent various beneficial impressions

consisting of antidiabetes, anticancer, antiallergy, antimutagenesis, cardioprotection, and antiviral activities [20–22]. One of the beneficial methods for discovering proper medication against COVID-19 can be molecular docking approach. This method can analyze the conformation and orientation of molecular structures into the binding zones of a macromolecular object [23]. Many research works have been remarked on the application of molecular docking method to determine or foretell the drug-object binding tendency with the viral protease [24–32]. The color of natural anthocyanins is changeable with concentration of H^+ in the liquid medium including weak acidic (Fig.1).

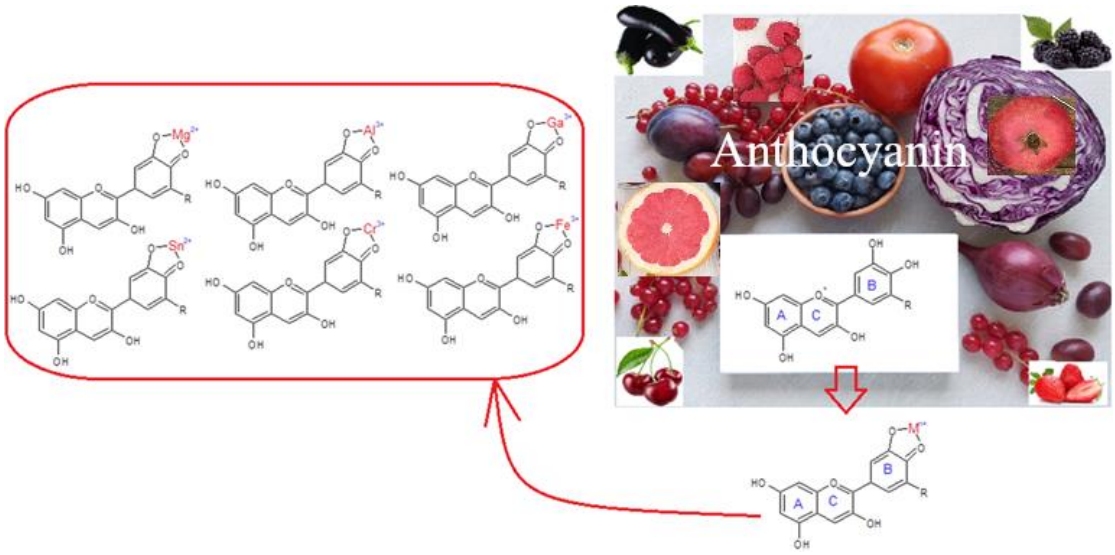

Fig. 1. Linkage of Mg^{2+}, Al^{3+}, Ga^{3+}, Sn^{2+}, Cr^{3+}, Fe^{3} to anthocyanins.

Antioxidants are extremely valuable food ingredients for our health as they fight against the famous free radicals, responsible for oxidative stress [33–35]. For example, the chelation of Al^{3+} by anthocyanins was more investigated owing to its dependence with the blue coloration of hydrangea floral structures. The complexes with acceptable stability between delphinidin and aluminum were found to produce acidified ethanol and a wide range of pH [36–39]. Phenolic plant seems to have multiple mechanisms of action in combating cancer including angiogenesis denying vascular tumors required for proliferation, inhibiting DNA synthesis, inducing apoptosis, and cellular differentiation inhibiting cancer progression. Regular consumption of raspberry anthocyanins is also reported to improve cognitive brain functions, age-related degeneration of eyesight and influence cardiovascular disease [40, 41].

Applying this approach, it can be remarked these dietary structures belong to the subclass of anthocyanin, which demonstrate the main ingredients in vegetables and fruits, as rich inhibiting agents of the main protease and targeting the receptor-binding domain (RBD) of S-protein for SARS-CoV2. In addition, molecular docking assigns swift diagnosis of the amino acid sequences for SARS-CoV-2 [42–44].

2. MATERIAL AND METHODS

Herein, comprehensive computational investigations were performed to identify new lead compounds against main protease enzyme. Geometry optimization of Mg^{2+}Cya, Al^{3+}Cya, Ga^{3+}Cya, Sn^{2+}Cya, Cr^{3+}Cya, and Fe^{3+}Cya chelation complexes through their B ring in water at 300K have been calculated using Gaussian 16 revision C.01 program [45]. In addition, the properties of Bader charge and thermodynamic parameters of Mg^{2+}ACN, Al^{3+}ACN, Ga^{3+}ACN,

Sn^{2+}ACN, Cr^{3+}ACN, and Fe^{3+}ACN chelation through their B ring in aqueous medium at 300K have been computed (Fig. 2 a, b, c).

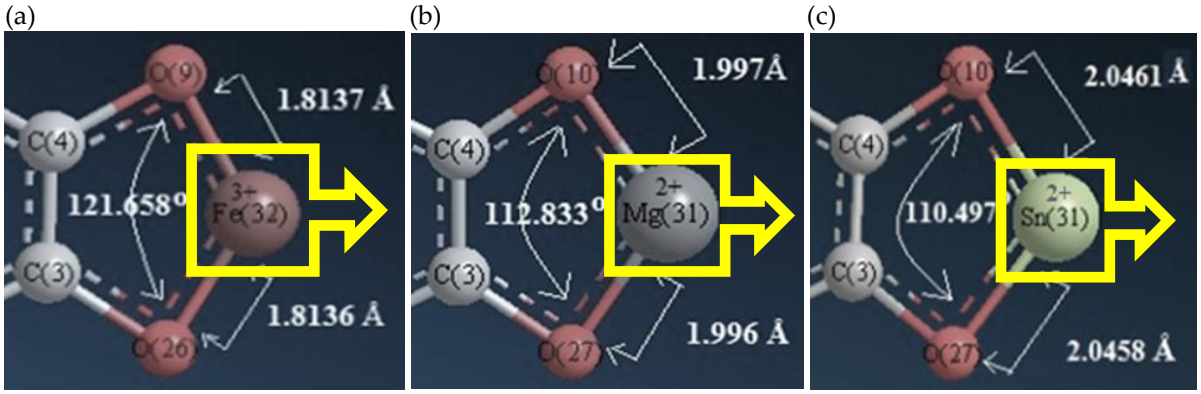

Fig. 2. Optimized structures of **(a)** Fe^{3+}ACN, **(b)** Mg^{2+}ACN, **(c)** Sn^{2+}ACN through remarking O ⋯ M^{n+} and bond angle of O ⋯ M^{n+} ⋯ O bond lengths.

For accomplishing a stable structure of Mg^{2+}ACN, Al^{3+}ACN, Ga^{3+}ACN, Sn^{2+}ACN, Cr^{3+}ACN, and Fe^{3+}ACN chelation of Mal, Peo, Del, Pet, and Cya pigments, geometry optimization plus frequency calculations were done; the frequency and intensity of the vibrational modes were calculated with the QM theoretical method, and the principal vibrational modes were analyzed by their changes of Gibbs free energy in water at 300K. The data has been achieved from thermodynamic parameters of ΔG, ΔH and ΔS for the solute-solvent model of Mg^{2+}ACN, Al^{3+}ACN, Ga^{3+}ACN, Sn^{2+}ACN, Cr^{3+}ACN, and Fe^{3+}ACN chelation. Thus, geometry coordination, Bader charge and thermodynamic attributes of three Al^{3+}→anthocyanin chelation of Cy, Dp, and Pt pigments through their B ring in gas and aqueous media at 300K have been estimated in a periodic box of H_2O molecules.

The optimized geometries include the bond length of oxygen - Mg^{2+} ≈ (1.9Å) and the bond angle of oxygen - Mg^{2+} - oxygen ≈ (112°) while it has been exhibited the bond length of oxygen - M^{3+} ≈ (1.8Å) and bond angle of oxygen - M^{3+} - oxygen ≈ (120°) for trivalent metal ions of Mg^{2+}, Al^{3+}, Ga^{3+}, Sn^{2+}, Cr^{3+} and Fe^{3+}. Our computations have been carried out due to the conceptual DFT/B3LYP/6–31G (d,p) method using the projector– augmented–wave (PAW) methodology [46–49]. The theoretical computations have been run to attain more valid equilibrium geometrical data and infrared spectral information for each of the recognized complexes.

3. RESULTS AND DISCUSSION

In this study, the candidate anthocyanin-derived compounds were filtered considering antiviral characteristics of anthocyanins. The structure-based pharmacophore modeling was developed based on the co-crystallized structure of the enzyme with its biological active inhibitor [50–52]. The thermodynamic properties including ΔG, ΔH, ΔS, Electronic Energy and Core-Core for conjunction of Mal, Peo, Del, Pet, and Cya with cations of Mg^{2+}, Al^{3+}, Ga^{3+}, Sn^{2+}, Cr^{3+}, Fe^{3+} in different pH have been measured using Gaussian 16 revision C.01 [45] program in aqueous medium (Table 1).

Table 1. Thermochemical specifications for Cya, Del, Mal, Pel, Peo, pet in aqueous medium at 300 K.

Pigment	$\Delta H \times 10^{-3}$ (kcal/mol)	$\Delta G \times 10^{-5}$ (kcal/mol)	$E_{binding}$ [53] (kcal/mol)	$\Delta S \times 10^{-2}$	$E_{electronic} \times 10^{-6}$ (kcal/mol)	$E_{core\text{-}core} \times 10^{-6}$ (kcal/mol)	ln $K \times 10^{-5}$
Cya	–1.54	–2.85	–6.4	9.44	–2.80	2.51	2.85
Del	–1.57	–2.92	–6.5	9.69	–2.89	2.60	4.90
Mal	–9.07	–2.11	–6.4	7.00	–1.86	1.65	3.54
Pel	–1.26	–2.45	–6.9	8.14	–2.25	2.01	1.37
Peo	–1.42	–2.72	–6.4	9.03	–2.61	2.33	4.56
Pet	–1.47	–2.80	-	9.28	–2.75	2.47	4.69

The difference of ΔH (kcal/mol) among the chelated complexes of Mg^{2+}ACN, Al^{3+}ACN, Ga^{3+}ACN, Sn^{2+}ACN, Cr^{3+}ACN, and Fe^{3+}ACN (Fig. 3) has been observed owing to double bonds and carbonyl groups through the chelation of B ring for Cya, Del and Pet anthocyanins in water that illustrates the stability and color of Mg^{2+}ACN, Al^{3+}ACN, Ga^{3+}ACN, Sn^{2+}ACN, Cr^{3+}ACN, and Fe^{3+}ACN chelation of Cya, Del, and Pet pigments in a weak acidic condition. The consequences of ΔH for formation of [Mg^{2+}, Al^{3+}, Ga^{3+}, Sn^{2+}, Cr^{3+}, Fe^{3+} → Cya, Del, Pet] chelation complexes have been shown by Fig.3 and reported data in Table 1.

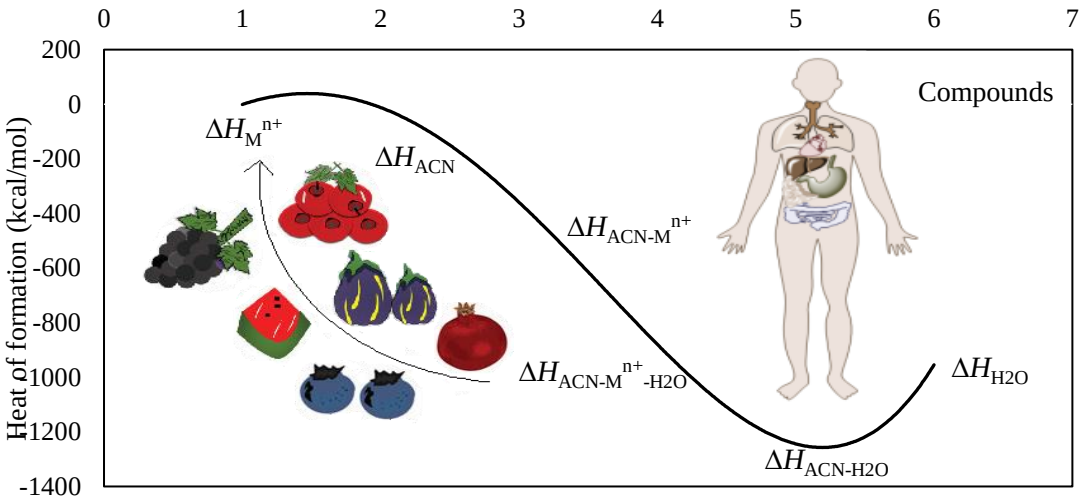

Fig. 3. Enthalpy reaction (Δ*H*, kcal/mol) for formation of Mg^{2+} ACN, Al^{3+}ACN, Ga^{3+}ACN, Sn^{2+}ACN, Cr^{3+}ACN, and Fe^{3+}ACN complexes.

After identifying all steps of the cation trapping reaction and the associated energy features, the overall Gibbs free energy profile was analyzed and shown in Table 1. The reactions in protons had to be fitted due to computational difficulty on the dissolution free energy of the proton. The effect of metal ions of Mg^{2+}, Al^{3+}, Ga^{3+}, Sn^{2+}, Cr^{3+}, Fe^{3+} joined to anthocyanins, which was modeled as an aqueous food system, was illustrated using thermodynamic computation. The equilibrium constant and free energy of the binding reaction between anthocyanins and stabilizers were theoretically important. The change in free energy change (Δ*G*) may be the best indicator of the protection offered by dietary stabilizers on anthocyanins, which was demonstrated the best stabilizer among dietary compounds as Del with $\Delta G = -2.92 \times 10^{-5}$ kcal/mol (Table 1).

Recently, it was evaluated the ability of eighteen compounds derived from anthocyaninin for the inhibition of the main protease (6lu7) and the receptor-binding domain of spike glycoprotein of SARS-CoV-2 [53]. Cyanidin-3-arabinoside exhibited significant binding stability and interaction, with key residues within the binding site of coronavirus main protease (6lu7). According to their study, the ligand cyanidin-3-arabinoside, which shows potential inhibition of SARS-COV-2 *in silico*, was observed in high concentration in *black chokeberries*, *bilberries*, *lingonberries*, *gooseberries*, *rubus*, *blackcurrants*, while pelargonidin-3-glucoside found in *raspberry* and *strawberry*. Therefore, they can prevent virus infection. Depending on the docking scores and binding energies, Cyanidin-3-arabinoside exhibits docking scores of −7.5 and −5.5 kcal/mol, so it is a potential inhibitor for SARS-CoV-2. Considering the achieved results, regular consumption of berry fruits can inhibit and control COVID–19 disease by suppression of propagation and pathogenicity of SARS-CoV-2 [53].

The absorbance (*A*) of chelated cations including Mg^{2+}, Ga^{3+}, Cr^{3+}, Fe^{3+}, and Al^{3+} with Cya, Del, and Pet pigments in aqueous periodic box has been calculated through the beer-lambert law which is related to the concentration (c/ mol/L) of H^+ (Table 2). The data have been shown based on equation of $A = \log_{10}(I_o/I) = \varepsilon lc$, where *A* is the absorbance; *I*, intensity of current; ε, molar absorptivity coefficient and c, concentration of solution (Table 2).

Table 2. Measured absorbance (A), Frequency and Dipole moment of metal→anthocyanin chelation of Cya, Del, and Pet in various pH

pH	A	Frequency	Dipole	A	Frequency	Dipole	A	Frequency	Dipole	A	Frequency	Dipole	A	Frequency	Dipole
Cya	$Mg^{2+}\times10^{-3}$			$Ga^{3+}\times10^{-3}$			$Cr^{3+}\times10^{-3}$			$Fe^{3+}\times10^{-3}$			$Al^{3+}\times10^{-3}$		
1.17	0.10	3.922	3.05	0.25	3.925	18.65	0.22	3.926	9.94	0.13	3.925	0.25	0.25	3.924	18.65
1.30	1.20	3.927	3.24	1.32	3.925	16.74	0.96	3.931	8.39	1.06	3.926	1.32	1.32	3.925	16.74
1.40	1.21	3.927	1.53	0.64	3.926	16.35	0.65	3.926	10.31	0.95	3.926	0.64	0.64	3.926	16.35
1.48	1.89	4.014	5.27	1.87	4.008	13.82	0.68	3.926	8.59	1.19	3928	1.87	1.87	4.008	13.82
1.54	1.89	4.012	3.91	1.85	4.007	6.69	1.90	4.009	9.59	1.90	4.012	1.85	1.85	4.007	6.69
Del pH	$Mg^{2+}\times10^{-3}$			$Ga^{3+}\times10^{-3}$			$Cr^{3+}\times10^{-3}$			$Fe^{3+}\times10^{-3}$			$Al^{3+}\times10^{-3}$		
1.17	0.70	3.926	6.71	0.42	3.925	18.78	0.89	3.933	9.04	0.89	3.767	7.90	3.59	3.925	16.19
1.30	1.20	3.929	3.67	1.25	3.927	14.94	0.89	3.933	9.04	3.93	3.945	7.47	1.07	3.929	17.15
1.40	2.81	5.816	2.60	1.24	3.928	12.99	1.07	3.935	6.40	0.89	3.928	6.87	1.12	3.929	16.10
1.48	1.24	3.930	4.91	3.75	4.041	15.99	1.92	4.018	7.38	1.92	4.018	5.54	1.86	4.015	17.01
1.54	1.92	4.018	3.75	1.90	4.014	13.14	1.84	4.015	9.03	1.95	4.016	6.38	1.80	4.013	16.86
Pet pH	$Mg^{2+}\times10^{-3}$			$Ga^{3+}\times10^{-3}$			$Cr^{3+}\times10^{-3}$			$Fe^{3+}\times10^{-3}$			$Al^{3+}\times10^{-3}$		
1.2	0.39	3.925	8.2	0.61	3.926	17.77	1.47	3.767	26.67	0.39	3.925	8.2	1.22	3.764	17.84
1.30	3.59	3.925	7.89	0.57	3.926	16.37	0.27	3.926	9.77	3.59	3.925	7.89	3.59	3.930	16.22
1.40	0.97	3.938	6.59	1.04	3.936	15.78	1.02	3.945	9.34	0.97	3.938	6.59	8.50	7.744	19.27
1.48	0.96	3.941	5.34	1.07	3.935	17.38	0.86	3.940	6.89	0.96	3.941	5.34	1.06	3.954	16.27
1.54	1.00	3.940	6.52	1.89	4.014	12.82	0.92	3.943	6.21	1.00	3.941	6.52	1.96	4.013	15.92

The reduction in absorbance might be related to reduced solubility of M^{n+}→ACN complexes which eventuate in precipitation of some complexes. The large increments in absorbance might be treated to convert as the colorless forms of ACN to those which absorb and reflect visible light as well as the M^{n+} induced linked to ACN compounds (Fig. 4 a,b). Furthermore,

the complexes of Ga^{3+}Pet, Cr^{3+}Pet, Mg^{2+} Pet (Fig. 4a) and Al^{3+}Cya, Ga^{3+}Cya, Mg^{2+}Cya (Fig. 4b) have indicated the maximum absorbance in the low concentration.

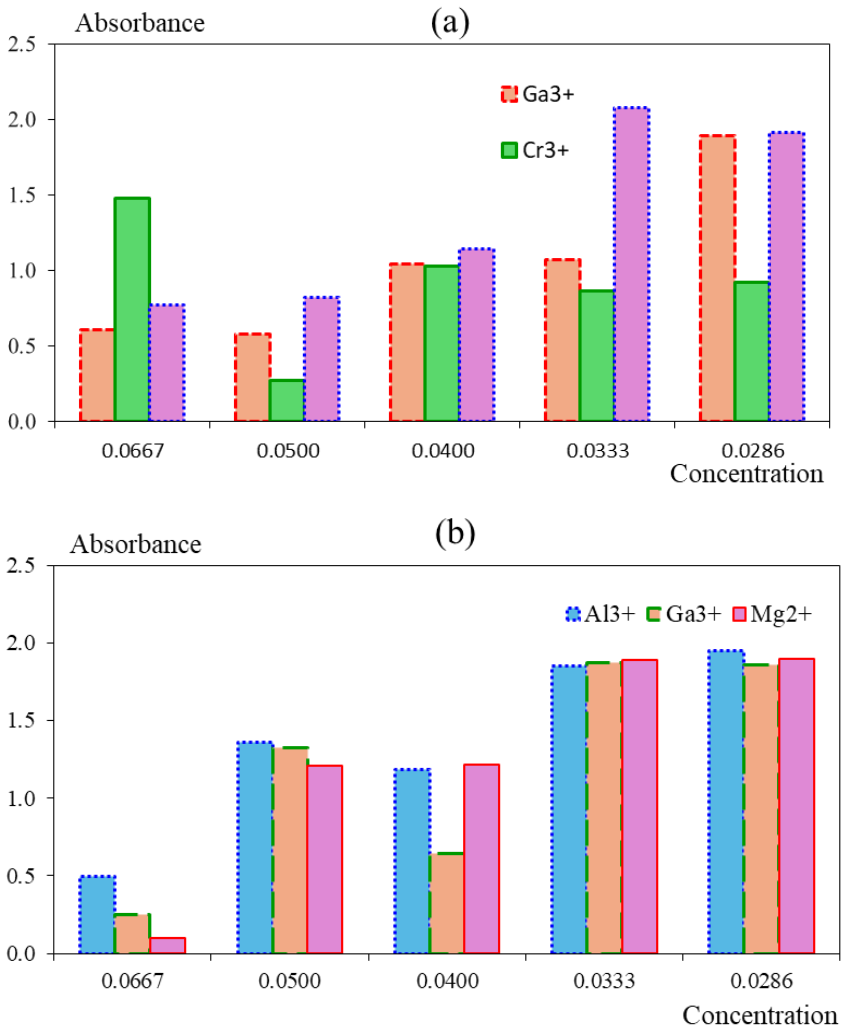

Fig. 4. The graphs of Absorbance versus concentration for complexes of **(a)** Ga^{3+}Pet, Cr^{3+}Pet, Mg^{2+}Pet and **(b)** Al^{3+}Cya, Ga^{3+}Cya, Mg^{2+}Cya complexes.

In all pH, the frequency, intensity, absorbance, and thermodynamics specifications of ACN-chelation were found to be significantly different with each metal treatment (Al^{3+}, Ga^{3+}, Mg^{2+}). In calculations, Al^{3+} was identified to displace Mg^{2+} in Mg^{2+}ACN complexes, Cya based and produces more stable complexes (Table 2). The nucleophilic index and dipole moment in different pH were applied to quantify van der Waals interaction between anthocyanins and stabilizers. It has been seen that by increasing the pH, the frequency of Al^{3+}Cya, Ga^{3+}Cya, Mg^{2+}Cya complexes increase between pH ≈1.1-1.5. The maximum frequency for Al^{3+}Cya, Ga^{3+}Cya, Mg^{2+}Cya complexes is in the pH between 1.50 to 1.55 of weak acidic medium (Table2). The frequency vibrational modes were indicated based on the stability and color of different cations→anthocyanin chelation (Table 2). Then, the Bader charge of indicated atoms in Mg^{2+}ACN, Ga^{3+}ACN, Cr^{3+}ACN, Fe^{3+}ACN, and Al^{3+}ACN chelation has been measured as the active zones of the structures which represent a significant function for the electron charge transfer towards generating a range of different colors in aqueous medium (Table 3).

Table 3. Bader charge for some particles of Mg^{2+} ACN, Ga^{3+}ACN, Cr^{3+}ACN, Fe^{3+}ACN, and Al^{3+}ACN in aqueous medium.

Cyanidin					
atom	Mg^{2+}	Ga^{3+}	Cr^{3+}	Fe^{3+}	Al^{3+}
O (10)	–0.42	–0.37	–0.02	–0.16	–0.36
O^{+} (17)	–0.13	–0.16	–0.13	–0.14	–0.13
O (24)	–0.20	–0.23	–0.21	–0.21	–0.18
O (25)	–0.22	–0.22	–0.21	–0.22	–0.21
O (26)	–0.21	–0.21	–0.21	–0.21	–0.21
O (27)	–0.39	–0.34	–0.07	–0.13	–0.33
M^{n+}(31)	0.76	0.76	0.45	0.07	0.02
Delphinidin					
atom	Mg^{2+}	Ga^{3+}	Cr^{3+}	Fe^{3+}	Al^{3+}
O (9)	–0.39	–0.56	0.0	–0.14	–0.32
O^{+}(16)	–0.13	–0.13	–0.13	–0.13	–0.13
O (23)	–0.20	–0.18	–0.21	–0.20	–0.18
O (24)	–0.21	–0.20	–0.20	–0.21	–0.20
O (25)	–0.21	–0.21	–0.21	–0.21	–0.21
O (26)	–0.40	–0.63	–0.06	–0.12	–0.33
O (30)	–0.21	–0.18	–0.21	–0.21	–0.19
M^{n+}(32)	0.76	0.64	0.42	0.04	0.04
Petunidin					
atom	Mg^{2+}	Ga^{3+}	Cr^{3+}	Fe^{3+}	Al^{3+}
O^{+}(7)	–0.13	–0.13	–0.13	–0.13	–0.13
O (17)	–0.40	–0.57	–0.03	–0.13	–0.33
O (18)	–0.39	–0.63	–0.04	–0.17	–0.33
O (19)	–0.20	–0.19	–0.21	–0.21	–0.19
O (20)	–0.21	–0.19	–0.21	–0.20	–0.21
O (21)	–0.22	–0.21	–0.22	–0.22	–0.21
O (30)	–0.15	–0.12	–0.15	–0.15	–0.13
M^{n+}(35)	0.76	0.65	0.42	0.0	0.03

The IR vibrational frequencies have shown that the normal mode of the active zones owing to cations→anthocyanin chelation of Al^{3+}Cya, Al^{3+}Del, and Al^{3+}Pet in optimized weak acidic media affirms the stability and color of these compounds. The alteration of Bader charge for functionalized atoms through optimized complexes of Mg^{2+}ACN, Al^{3+}ACN, Ga^{3+}ACN, Sn^{2+}ACN, Cr^{3+}ACN, and Fe^{3+}ACN have been plotted in Fig. 5(a, b).

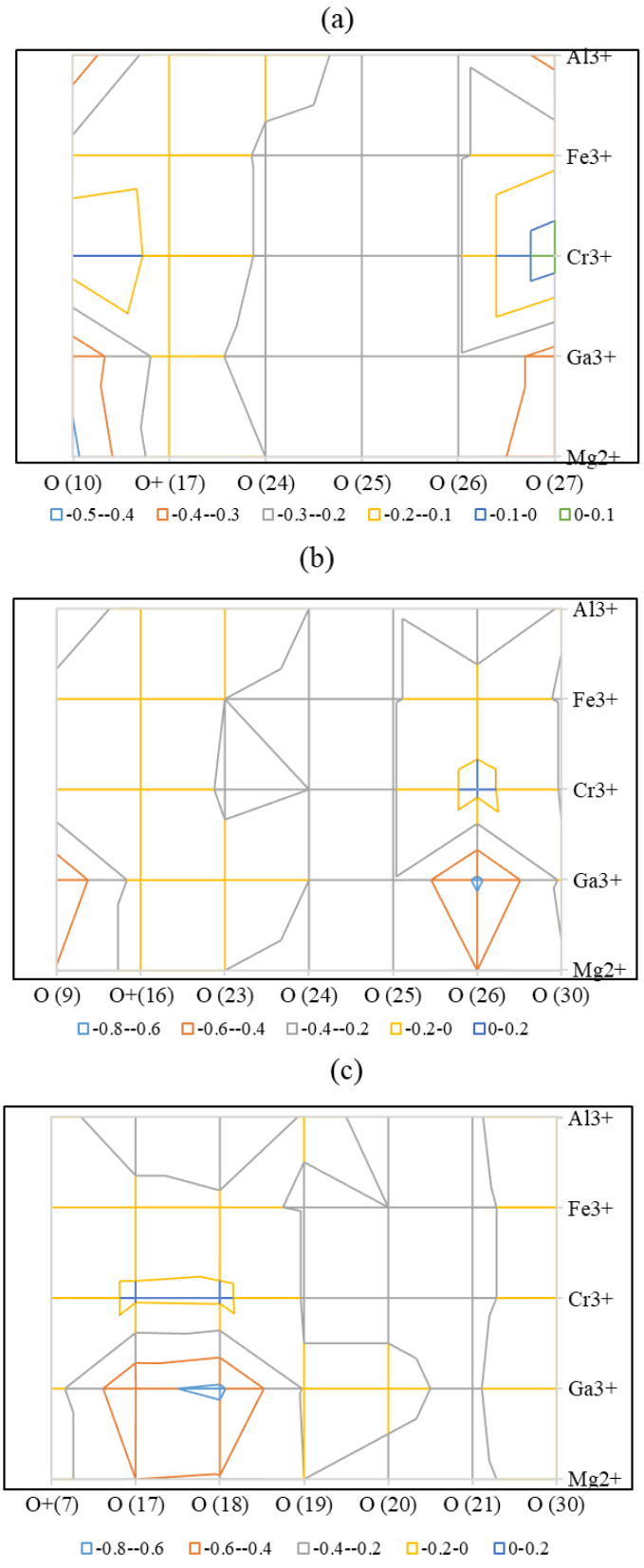

Fig. 5. Atomic orbital electron population for some atoms through optimized Mg^{2+} ACN, Al^{3+}ACN, Ga^{3+} ACN, Sn^{2+}ACN, Cr^{3+}ACN, and Fe^{3+}ACN chelation in aqueous medium.

As a matter of fact, the partial charges and spin density have been gained by matching the electrostatic potential to atomic charge of O^{+}_{17}, O^{+}_{16}, and O^{+}_{7} ions for M^{n+}(31)Cya, M^{n+}(32)Del

and M^{n+}(35)Pet, respectively (Table 3 & Fig. 5a,b). Thus, the electrophilic groups of Cya, Del anthocyanin pigments lead us to explore the cause for the activity and the stability of these compounds in natural products. The perspective of Fig. 5(a,b) suggests the cause for observing a variety of consequences for chelated complexes of Mg^{2+}ACN, Al^{3+}ACN, Ga^{3+}ACN, Sn^{2+}ACN, Cr^{3+}ACN, and Fe^{3+}ACN which are attached to the location of active zones of functionalized oxygen atoms and cations in these structures due to charge transferring in aromatic cyclic chain.

CONCLUSIONS

The receptor–ligand complexes of the lead compounds were analyzed, and a hypothesis was generated using the phase interface of DFT method to highlight the major properties that actively contribute to the characteristic binding of the lead ligands to the active sites of the target proteins. This study evaluates the ability of these compounds for inhibiting the main protease and the receptor–binding domain of spike glycoprotein of SARS-CoV-2 through molecular modeling simulation. Applying beer-lambert proof on chelated complexes of Mg^{2+}ACN, Al^{3+}ACN, Ga^{3+}ACN, Sn^{2+}ACN, Cr^{3+}ACN, and Fe^{3+}ACN using theoretical approaches indicates absorbance factor in gas and aqueous media and then explores the stabilization energy, thermodynamic specifications and the electronic structural of optimized cluster chelated of Mg^{2+}ACN, Al^{3+}ACN, Ga^{3+}ACN, Sn^{2+}ACN, Cr^{3+}ACN, and Fe^{3+}ACN. In addition, it has been discovered that [Mg^{2+}, Al^{3+}, Ga^{3+}, Sn^{2+}, Cr^{3+} and Fe^{3+}→ anthocyanin] cluster chelation is related to the axes of active areas of functionalized oxygen atoms and cations in these complexes which alter the electronic charges in aromatic cyclic chains because of aqueous dielectric constant compered to gas medium. Regarding the received results, regular consumption of some vegetables and fruits could be useful to monitor and inhibit COVID–19 disease by suppression of propagation and pathogenicity of SARS-CoV-2.

ACKNOWLEDGMENTS

In successfully completing this paper and its research, the authors are grateful to Kastamonu University.

CONFLICTS OF INTEREST

The authors declare no conflict of interest.

REFERENCES

1. L. Alomair, S. Mustafa, M.S. Jafri, W. Alharbi, A. Aljouie, F. Almsned M. Alawad, Y.A. Bokhari & M. Rashid. Molecular dynamics simulations to decipher the role of phosphorylation of SARS-CoV-2 nonstructural proteins (nsps) in viral replication. *Viruses*, **14**(11), 2436 (2022). Doi: https://doi.org/10.3390/v14112436
2. M.A.A. Zadeh, H. Lari, L. Kharghanian, E. Balali, R. Khadivi, H. Yahyaei, F. Mollaamin & M. Monajjemi. Density functional theory study and anti-cancer properties of Shyshaq plant: In view point of nano biotechnology. *J. Comput. Theoret. Nanosci.*, *12*(11), 4358-4367 (2015). Doi: https://doi.org/10.1166/jctn.2015.4366
3. M. Monajjemi, S. Afsharnezhad, M.R. Jaafari, S. Mirdamadi, F. Mollaamin & H. Monajemi. Investigation of energy and NMR isotropic shift on the internal rotation Barrier of Θ4 dihedral angle of the DLPC: A GIAO study. *Chemistry*, **17**(1), 55–69 (2008).

4. M. Monajjemi, F. Mollaamin & S. Shojaei. An overview on coronaviruses family from past to COVID-19: Introduce some inhibitors as antiviruses from Gillan's plants. *Biointerface Res. Appl. Chem.*, **10**(3), 5575–5585 (2020). Doi: https://doi.org/10.33263/briac103.575585
5. S. Shahriari, M. Monajjemi & F. Mollaamin. Determination of proteins specification with SARS-Covid-19 based ligand designing. *J. Chil. Chem. Soc.*, **67**(2), 5468–5476 (2022). Doi: https://doi.org/10.4067/s0717-97072022000205468
6. A. Majeed & X. Zhang. On the adoption of modern technologies to fight the COVID-19 pandemic: A technical synthesis of latest developments. COVID, **3**(1), 90–123 (2023). Doi: https://doi.org/10.3390/covid3010006
7. F. Mollaamin. Conocimiento de enfermedades virales terapéuticas: aplicación de SWCNT en la administración de fármacos. *Rev. Colomb. Quím.*, **52**(2), 28–35 (2024). Doi: https://doi.org/10.15446/rev.colomb.quim.v52n2.111888
8. F. Mollaamin. Characterizing the structural and physicochemical properties of medicinal plants as a proposal for treating of viral malady. *Trends Immunother.*, **7**(2), 2329 (2023). Doi: https://doi.org/10.24294/ti.v7.i2.2329
9. F. Mollaamin & M. Monajjemi. Thermodynamic research on the inhibitors of coronavirus through drug delivery method. *J. Chil. Chem. Soc.*, **66**(2), 5195–5205 (2021). Doi: https://doi.org/10.4067/s0717-97072021000205195
10. A. Tahan, F. Mollaamin & M. Monajjemi. Thermochemistry and NBO analysis of peptide bond: Investigation of basis sets and binding energy. *Russ. J. Phys. Chem. A*, **83**(4), 587–597 (2009). Doi: https://doi.org/10.1134/S003602440904013X
11. F. Mollaamin. Structural and functional characterization of medicinal plants as selective antibodies towards therapy of COVID-19 symptoms. *Antibodies*, **13**(2), 38 (2024). Doi: https://doi.org/10.3390/antib13020038
12. F. Zeng, Y. Huang, Y. Guo, M. Yin, X. Chen, L. Xiao & G. Deng. Association of inflammatory markers with the severity of COVID-19: A meta-analysis. *Int. J. Infect. Dis.*, 96, 467–474 (2020). Doi: https://doi.org/10.1016/j.ijid.2020.05.055
13. F. Mollaamin. Physicochemical investigation of anti-covid19 drugs using several medicinal plants. *J. Chil. Chem. Soc.*, **67**(2), 5537–5546 (2022). Doi: https://doi.org/10.4067/s0717-97072022000205537
14. Q.M.S. Jamal. Antiviral potential of plants against COVID-19 during outbreaks—An update. *Int. J. Mol. Sci.*, **23**(21), 13564 (2022). Doi: https://doi.org/10.3390/ijms232113564
15. J. Remali & W.M. Aizat. A review on plant bioactive compounds and their modes of action against coronavirus infection. *Front. Pharmacol.*, **11**, 589044 (2021). Doi: https://doi.org/10.3389/fphar.2020.589044
16. F. Mollaamin, S. Shahriari & M. Monajjemi. Monkeypox disease treatment by tecovirimat adsorbed onto single-walled carbon nanotube through drug delivery method. *J. Chil. Chem. Soc.*, **68**(1), 5796–5801 (2023). Doi: https://doi.org/10.4067/s0717-97072023000105796
17. T. Capell, R.M. Twyman, V. Armario-Najera, J.K.-C. Ma, S. Schillberg & P. Christou. Potential applications of plant biotechnology against SARS-CoV-2. *Trends Plant Sci.*, **25**(7), 635–643 (2020). Doi: https://doi.org/10.1016/j.tplants.2020.04.009
18. F. Mollaamin & M. Monajjemi. B_5N_{10} Nanocarrier functionalized with Al, C, Si atoms: A drug delivery method for infectious disease remedy. *OBM Genetics*, **08**(01), 214 (2024). Doi: https://doi.org/10.21926/obm.genet.2401214
19. S. Murugesan, C. Ragavendran, A. Ali, V. Arumugam, D.K. Lakshmanan, P. Palanichamy, *et al.* Screening and druggability analysis of marine active metabolites against SARS-CoV-2: An integrative computational approach. *Int. J. Transl. Med.*, 3(1), 27–41 (2022). Doi: https://doi.org/10.3390/ijtm3010003
20. M.L. Castro-Acosta, G.N. Lenihan-Geels, C.P. Corpe & W.L. Hall. Berries and anthocyanins: promising functional food ingredients with postprandial glycaemia-lowering effects. *Proc. Nutr. Soc.*, **75**(3), 342–355 (2016). Doi: https://doi.org/10.1017/s0029665116000240
21. O. Paredes-López, M.L. Cervantes-Ceja, M. Vigna-Pérez & T. Hernández-Pérez. Berries: Improving human health and healthy aging, and promoting quality life—A review. *Plant Foods Hum. Nutr.*, **65**(3), 299–308 (2010). Doi: https://doi.org/10.1007/s11130-010-0177-1

22. F. Mollaamin & M. Monajjemi. Drug delivery using doping of boron nitride nanosensor towards releasing chloroquine drug in the cells: A promising method for overcoming viral disease. *Rev. Colomb. Cienc. Quím. Farm.*, **53**(2), 430–454 (2024). Doi: https://doi.org/10.15446/rcciq-uifa.v53n2.114450
23. P.H.M. Torres, A.C.R. Sodero, P. Jofily & F.P. Silva, Jr. Key topics in molecular docking for drug design. *Int. J. Mol. Sci.*, **20**(18), 4574 (2019). Doi: https://doi.org/10.3390/ijms20184574
24. S. Das, S. Sarmah, S. Lyndem & A.S. Roy. An investigation into the identification of potential inhibitors of SARS-CoV-2 main protease using molecular docking study. *J. Biomol. Struct. Dyn.*, **39**(9), 3347–3357 (2021). Doi: https://doi.org/10.1080/07391102.2020.1763201
25. M. Monajjemi, A. Sobhanmanesh & F. Mollaamin. Theoretical studies of solvent effects on binding of $Sn(CH_3)_2$(N-acetyl-L-cysteinate) with single-walled carbon nanotube. *Fuller. Nanotub. Carbon Nanostruct.*, **21**(1), 47–63 (2013). Doi: https://doi.org/10.1080/1536383X.2011.574325
26. P.T. Mpiana, K.t.N. Ngbolua, D.S.T. Tshibangu, J.T. Kilembe, B.Z. Gbolo, D.T. Mwanangombo, C.L. Inkoto, E.M. Lengbiye, C.M. Mbadiko, A. Matondo, G.N. Bongo & D.D. Tshilanda. Identification of potential inhibitors of SARS-CoV-2 main protease from Aloe vera compounds: A molecular docking study. *Chem. Phys. Lett.*, **754**, 137751 (2020). Doi: https://doi.org/10.1016/j.cplett.2020.137751
27. B. Khalili-Hadad, F. Mollaamin & M. Monajjemi. Biophysical chemistry of macrocycles for drug delivery: a theoretical study. *Russ. Chem. Bull.*, **60**(2), 238–241 (2011). Doi: https://doi.org/10.1007/s11172-011-0039-5
28. F. Mollaamin & M. Monajjemi. Thermodynamic research on the inhibitors of coronavirus through drug delivery method. *J. Chil. Chem. Soc.*, **66**(2), 5195–5205 (2021). Doi: https://doi.org/10.4067/s0717-97072021000205195
29. S. Mazzini, L. Musso, S. Dallavalle & R. Artalli. Putative SARS-CoV-2 Mpro inhibitors from an in-house library of natural and nature-inspired products: A virtual screening and molecular docking study. *Molecules*, **25**(16), 3745 (2020). Doi: https://doi.org/10.3390/molecules25163745
30. F. Mollaamin & M. Monajjemi. Molecular drug discovery of potential inhibitor of Covid–19 using several medicinal plant ingredients: A promising therapy for viral disease. *Rev. Fac. Cienc.*, **13**(1), 141–158 (2024). doi: https://doi.org/10.15446/rev.fac.cienc.v13n1.111288
31. M. Alfaro, I. Alfaro & C. Angel. Identification of potential inhibitors of SARS-CoV-2 papain-like protease from tropane alkaloids from *Schizanthus porrigens*: A molecular docking study. *Chem. Phys. Lett.*, **761**, 138068 (2020). Doi: https://doi.org/10.1016/j.cplett.2020.138068
32. F. Mollaamin. Computational methods in the drug delivery of carbon nanocarriers onto several compounds in Sarraceniaceae medicinal plant as monkeypox therapy. *Computation*, **11**(4), 84 (2023). Doi: https://doi.org/10.3390/computation11040084
33. M.E. Olsson, K.E. Gustavsson, S. Andersson, Å. Nilsson & R.-D. Duan. Inhibition of cancer cell proliferation *in vitro* by fruit and berry extracts and correlations with antioxidant levels. *J. Agricul. Food Chem.*, **52**(24), 7264–7271 (2004). Doi: https://doi.org/10.1021/jf030479p
34. F. Mollaamin & M. Monajjemi. Application of DFT/TD-DFT frameworks in the drug delivery mechanism: Investigation of chelated bisphosphonate with transition metal cations in bone treatment. *Chemistry*, **5**(1), 365–380 (2023). Doi: https://doi.org/10.3390/chemistry5010027
35. B. Ghalandari, M. Monajjemi & F. Mollaamin. Theoretical investigation of carbon nanotube binding to DNA in view of drug delivery. *J. Comput. Theor. Nanosci.*, **8**(7), 1212–1219 (2011). Doi: https://doi.org/10.1166/jctn.2011.1801
36. F. Mollaamin, S. Shahriari & M. Monajjemi. Treating omicron BA.4 & BA.5 via herbal antioxidant asafoetida: A DFT study of carbon nanocarrier in drug delivery. *J. Chil. Chem. Soc.*, **68**(1), 5781–5786 (2023). Doi: https://doi.org/10.4067/S0717-97072023000105781
37. E.M. Sarasia, S. Afsharnezhad, B. Honarparvar, F. Mollaamin & M. Monajjemi. Theoretical study of solvent effect on NMR shielding tensors of luciferin derivatives. *Phys. Chem. Liq.*, **49**(5), 561–571 (2011). Doi: https://doi.org/10.1080/00319101003698992
38. F. Mollaamin & M. Monajjemi. Determination of SWCNT biosensor for bisphosphonate–2X (X = Mg^{2+}, Ca^{2+}, Sr^{2+}) delivery in bone cell through electromagnetic and thermodynamic analysis using QM/MC methods. *Sensor Rev.*, **44**(2), 100–112 (2024). Doi: https://doi.org/10.1108/SR-05-2023-0148

39. M. Monajjemi, H. Yamola & F. Mollaamin. Study of bio-nano interaction outlook of amino acids on single-walled carbon nanotubes. *Fuller. Nanotub. Carbon Nanostruct.*, **22**(6), 595–603 (2014). Doi: https://doi.org/10.1080/1536383X.2012.702163
40. H.D. Schreiber, A.M. Swink & T.D. Godsey. The chemical mechanism for Al^{3+} complexing with delphinidin: A model for the bluing of hydrangea sepals. *J. Inorg. Biochem.*, **104**(7), 732–739 (2010). Doi: https://doi.org/10.1016/j.jinorgbio.2010.03.006
41. F. Mollaamin & M. Monajjemi. Carbon nanotubes as biosensors for releasing conjugated bisphosphonates–metal ions in bone tissue: Targeted drug delivery through the DFT Method. *C J. Carbon Res.*, **9**(2), 61 (2023). Doi: https://doi.org/10.3390/c9020061
42. F. Mollaamin, S. Shahriari & M. Monajjemi. Therapeutic role of medicinal plants against viral diseases focusing on COVID-19: Application of computational chemistry towards drug design. *Rev. Colomb. Cienc. Quím. Farm.*, **53**(1), 19–43 (2024). Doi: https://doi.org/10.15446/rcciquifa.v53n1.112978
43. K.N. Chitrala, X. Yang, B. Busbee, N.P. Singh, L. Bonati, Y. Xing, P. Nagarkatti & M. Nagarkatti. Computational prediction and in vitro validation of VEGFR1 as a novel protein target for 2,3,7,8-tetrachlorodibenzo-p-dioxin. *Sci. Reports*, **9**(1), 6810 (2019). Doi: https://doi.org/10.1038/s41598-019-43232-4
44. F. Mollaamin, S. Shahriari & M. Monajjemi. Drug design of medicinal plants as a treatment of Omicron variant (Covid-19 variant B.1.1.529). *J. Chil. Chem. Soc.*, **67**(3), 5562–5570 (2022). Doi: https://doi.org/10.4067/s0717-97072022000305562
45. M.J. Frisch, G.W. Trucks, H.B. Schlegel, G.E. Scuseria, M.A. Robb, J.R. Cheeseman, *et al.* Gaussian 16, Revision C.01, Gaussian, Inc., Wallingford CT, 2016.
46. A.D. Becke. Density-functional thermochemistry. III. The role of exact exchange. *J. Chem. Phys.*, **98**(7), 5648–5652 (1993). Doi: https://doi.org/10.1063/1.464913
47. J.P. Perdew, M. Ernzerhof & K. Burke. Rationale for mixing exact exchange with density functional approximations. *J. Chem. Phys.*, **105**(22), 9982–9985 (1996). Doi: https://doi.org/10.1063/1.472933
48. F. Mollaamin & M. Monajjemi. Molecular modelling framework of metal-organic clusters for conserving surfaces: Langmuir sorption through the TD-DFT/ONIOM approach. *Mol. Simulat.*, **49**(4), 365–376 (2023). Doi: https://doi.org/10.1080/08927022.2022.2159996
49. K. Bakhshi, F. Mollaamin & M. Monajjemi. Exchange and correlation effect of hydrogen chemisorption on nano V(100) surface: A DFT study by Generalized Gradient Approximation (GGA). *J. Comput. Theor. Nanosci.*, **8**, 763–768 (2011). Doi: https://doi.org/10.1166/jctn.2011.1750
50. D. Marko, N. Puppel, Z. Tjaden, S. Jakobs & G. Pahlke. The substitution pattern of anthocyanidins affects different cellular signaling cascades regulating cell proliferation. *Mol. Nutr. Food Res.*, **48**(4), 318–325 (2004). Doi: https://doi.org/10.1002/mnfr.200400034
51. N. Katsube, K. Iwashita, T. Tsushida, K. Yamaki & M. Kobori. Induction of apoptosis in cancer cells by bilberry (*Vaccinium myrtillus*) and the anthocyanins. *J. Agricult. Food Chem.*, **51**(1), 68–75 (2002). Doi: https://doi.org/10.1021/jf025781x
52. S. Zafra-Stone, T. Yasmin, M. Bagchi, A. Chatterjee, J.A. Vinson & D. Bagchi. Berry anthocyanins as novel antioxidants in human health and disease prevention. *Mol. Nutr. Food Res.*, **51**(6), 675–683 (2007). Doi: https://doi.org/10.1002/mnfr.200700002
53. O. Messaoudi, H. Gouzi, A.N. El-Hoshoudy, F. Benaceur, C. Patel, D. Goswami, D. Boukerouis & M. Bendahou. Berries anthocyanins as potential SARS-CoV–2 inhibitors targeting the viral attachment and replication; molecular docking simulation. *Egypt. J. Petroleum*, **30**(1), 33–43 (2021). Doi: https://doi.org/10.1016/j.ejpe.2021.01.001

HOW TO CITE THIS ARTICLE

F. Mollaamin & M. Monajjemi. Antiviral effect of anthocyanins in vegetables and fruits against viral diseases: Insight to medication design by computational chemistry approaches. *Rev. Colomb. Cienc. Quim. Farm.*, **54**(1), 218–230 (2025). Doi: https://doi.org/10.15446/rcciquifa.v54n1.119556